Biogeosciences Discuss., 10, 17549–17595, 2013
www.biogeosciences-discuss.net/10/17549/2013/
doi:10.5194/bgd-10-17549-2013

Biogeosciences Discussions
Open Access

Methyl iodide production in the open ocean

I. Stemmler[1,3], **I. Hense**[1], **B. Quack**[2], **and E. Maier-Reimer**[3]

[1]Institute for Hydrobiology and Fisheries Science, University of Hamburg, CEN, Hamburg, Germany
[2]Geomar, Helmholtz Centre for Ocean Research, Kiel, Germany
[3]Max Planck Institute for Meteorology, Hamburg, Germany

Received: 16 October 2013 – Accepted: 30 October 2013 – Published: 8 November 2013

Correspondence to: I. Stemmler (irene.stemmler@zmaw.de)

Published by Copernicus Publications on behalf of the European Geosciences Union.

Abstract

Production pathways of the prominent volatile organic halogen compound methyl iodide (CH_3I) are not fully understood. Previous model studies suggest either production via photochemical degradation of organic material or rather phytoplankton production. Correlations between biological and environmental variables derived from observations also suggest both production pathways. In this study we aim to address this question of source mechanisms with a global three-dimensional ocean general circulation model including biogeochemistry (MPIOM-HAMOCC) by carrying out a series of sensitivity experiments. Simulated distribution patterns and emissions of CH_3I differ largely for the different production pathways. However, the evaluation of our model results with observations from a newly available global data set shows that observed surface concentrations of CH_3I can be best explained by the photochemical production pathway. Our results further emphasize that correlations between CH_3I and abiotic or biotic factors do not necessarily provide meaningful insights concerning the source of origin. Overall, we find a net global annual CH_3I air–sea flux that ranges between 70 and 260 $Gg\,yr^{-1}$. Hence, at the global scale the ocean is a net source of methyl iodide for the atmosphere, though in some regions in boreal winter fluxes are of opposite direction (from the atmosphere to the ocean).

1 Introduction

Methyl iodide (CH_3I) is an organic halogen of natural origin. Following emission from the ocean (or land) it is photolysed within days to reactive iodine species that affect the oxidative capacity of the atmosphere (e.g via ozone depletion) (Chameides and Davis, 1980; Solomon et al., 1994; Rattigan et al., 1997; Vogt et al., 1999; Carpenter, 2003). CH_3I is ubiquitously detected in water and air in the marine boundary layer (e.g., Singh et al., 1983; Happell and Wallace, 1996; Chuck et al., 2005; Smythe-Wright et al., 2006; Butler et al., 2007; Fuhlbrügge et al., 2013). The strength of the CH_3I source

BGD
10, 17549–17595, 2013

to the atmosphere is estimated using different methods. Either it is derived from extrapolating fluxes diagnosed from concentrations measured during ship cruises (e.g., Moore and Groszko, 1999; Chuck et al., 2005; Butler et al., 2007; Jones et al., 2010; Ziska et al., 2013) or by analysing oceanic source and sink processes (e.g., Manley and De La Cuesta, 1997; Bell et al., 2002; Carpenter, 2003; Richter and Wallace, 2004; Youn et al., 2010). In this regard, several marine macroalgae have been identified as CH_3I producers (Gschwend et al., 1985; Nightingale et al., 1995; Itoh et al., 1997; Giese et al., 1999; Carpenter et al., 2000) and are thought to be the dominant source in the coastal ocean. In the open ocean, there is evidence for several production pathways: production through photochemical degradation of organic matter (e.g. Moore and Zafiriou, 1994; Richter and Wallace, 2004), production by marine biota (e.g., Smythe-Wright et al., 2006; Amachi, 2008; Karlsson et al., 2008; Brownell et al., 2010), or through substitution when dust contacts seawater containing iodide or when marine water vapor condenses on dust containing iodide (Williams et al., 2007). A common method is to deduce production pathways from covariation of CH_3I concentrations and abiotic and biotic proxy parameters. Observed CH_3I concentrations in seawater and marine air were correlated with phytoplankton biomass (Smythe-Wright et al., 2006), phytoplankton pigment concentrations (Abrahamsson et al., 2004; Chuck et al., 2005; Wang et al., 2009; Lai et al., 2011), temperatures (Rasmussen et al., 1982; Happell and Wallace, 1996; Yokouchi et al., 2001; Chuck et al., 2005; Wang et al., 2009), and radiation (Happell and Wallace, 1996; Chuck et al., 2005; Wang et al., 2009). Most of these studies suggested either the biological or the photochemical production pathway. Laboratory studies identify several phytoplankton species (e.g. *Nitzschia, Phaeocystis, Prochlorococcus, Synechococcus, Emiliania, Thalassiosira, Phaeodactylum*) (Moore and Tokarczyk, 1993; Hughes et al., 2006; Smythe-Wright et al., 2006; Brownell et al., 2010; Toda and Itoh, 2011) as CH_3I producers. Additionally, heterotrophic, non-photosynthesising bacteria (Manley and Dastoor, 1988; Manley, 1994; Amachi et al., 2001; Fuse et al., 2003; Amachi, 2008) decomposing detrital particles (Hughes et al., 2008) have been proposed to constitute significant biological sources of CH_3I. The

BGD
10, 17549–17595, 2013

photochemical production pathway has also been observed in laboratory experiments (e.g. Richter and Wallace, 2004). These methods, i.e. the extrapolation from ship-based measurements to global sources or emissions, and the extrapolation from laboratory to natural conditions include inherent uncertainties. On the one hand it is questionable whether phytoplankton cultivated under laboratory condition behaves like in the open ocean. On the other hand, measurements from field campaigns only reflect snapshots and it is unclear whether they can be used to identify possible production pathways.

Numerical models can help to reduce these uncertainties. They can be used to test different findings on production and to extrapolate consistently (based on process parameterizations) in space and time. Previous model studies have been conducted, but they also show contradicting evidence for a photochemical or a direct biological production pathway. Bell et al. (2002) and Youn et al. (2010) studied CH_3I originating from natural sources using a global atmospheric chemistry-transport model coupled to a mixed layer ocean model. Best agreement between observations and model results has been obtained when considering only a photochemical source instead of considering biological production (Bell et al. (2002) as well as Youn et al. (2010), who adopted the same parameterization). In a recent model study with a 1-D water-column model, Stemmler et al. (2013) assessed the relevance of different production pathways for representing observed CH_3I profiles in the tropical Atlantic Ocean. The results indicate, in contrast, that the vertical profile at Cape Verde is predominantly due to CH_3I production by phytoplankton. However, effects of horizontal and vertical advection have been neglected. The global model studies, on the other hand, could not make use of the recently established global data set for organic halogens (Ziska et al., 2013) and only relatively few observations for the evaluation were available. Thus, it is still unclear whether surface concentrations might or might not be best explained by direct biological or photochemical production. In the current study, we use this methyl iodide module within a global oceanic general circulation model, MPIOM-HAMOCC (Marsland et al., 2003; Ilyina et al., 2013) and the global dataset of CH_3I observations (Ziska et al., 2013) to re-address the question of different CH_3I production pathways. We also aim to ana-

BGD
10, 17549–17595, 2013

lyze relationships between CH_3I concentrations and biotic as well as abiotic variables in a similar way as it is done with field measurements to assess the interpretability of these correlations. Furthermore, we derive sea–air fluxes to investigate possible differences in CH_3I emissions due to different sources; the results will be compared with published emission estimates.

2 Material and methods

2.1 Model description

Methyl iodide modeling was performed with the ocean general circulation model MPIOM (Marsland et al., 2003) coupled to the marine carbon cycle model HAMOCC5.2 (Six and Maier-Reimer, 1996; Ilyina et al., 2013) and the CH_3I module presented in Stemmler et al. (2013). Methyl iodide cycling includes production, degradation, air–sea gas exchange, diffusion and advection. Two production mechanisms are resolved: direct biological production by phytoplankton, and photochemical production by radical recombination between methyl groups and iodine atoms. Biological production of CH_3I follows phytoplankton growth using either a constant or variable phytoplankton to methyl iodide production ratio. Photochemical production is parametrized linear to radiation and dissolved organic carbon concentration. CH_3I degradation includes nucleophilic substitution with chloride, hydrolysis, and photolysis. Degradation processes are described as first-order kinetics with temperature-dependent rates taken from literature (Elliott and Rowland, 1993, 1995; Rattigan et al., 1997). Gas exchange is calculated from the two-film model using a time-invariant field of atmospheric concentrations (see Sect. 2.3), the Schmidt number (Moore and Groszko, 1999) and a transfer velocity (Nightingale et al., 2000). A detailed description of process parameterizations and chemical properties of CH_3I can be found in Stemmler et al. (2013).

BGD
10, 17549–17595, 2013

2.2 Model setup

For this study the MPIOM version 1.5.0 was run in a horizontal resolution of approx. 1.5°(i.e. GR15L40). It uses a curvilinear grid with the North Pole shifted over Greenland. The model resolves 40 vertical levels of varying depths with a higher resolution in the upper, sun-lit ocean where primary production (PP) takes place.

Based on our insights from previous model experiments in which the production rates were optimized to best fit observed concentrations (Stemmler et al., 2013), we performed the following experiments (Table 1):

Opt1 "Normal" biological production: Stemmler et al. (2013) show that in the model experiment with optimized parameters for biological production the best agreement with observed profiles of CH_3I could be achieved. In particular, the model was able to reproduce the low surface concentration and a pronounced subsurface maximum. Therefore we adopt this experiment in which CH_3I is produced during phytoplankton growth using a constant production ratio.

Opt2 "Stressed" biological production: Stemmler et al. (2013) show that the consideration of enhanced production by physiologically stressed phytoplankton (i.e. the picocyanobacteria species *Prochlorococcus*) as suggested by Hughes et al. (2011) did not improve the model performance. However, due to several uncertainties as discussed in Stemmler et al. (2013) it cannot be excluded that this mechanism is important; we therefore consider this production pathway. In this experiment CH_3I is produced during phytoplankton growth using a production rate that varies in space and time depending on nutrient availability.

Opt3 Photochemical production from semi-labile dissolved organic carbon (SLDOC): Bell et al. (2002) state in their model study that best agreement between simulated and observed CH_3I surface concentrations is achieved when photochemical production using SLDOC is taken into account; we therefore follow their approach.

BGD
10, 17549–17595, 2013

In this experiment CH_3I production is linearly coupled to light and the dissolved organic carbon concentration provided by HAMOCC.

Opt4 Photochemical production from a constant surface DOC pool: model sensitivity experiments with photochemical production of semilabile (SLDOC) or refractory (RDOC) did not reveal significant differences (Stemmler et al., 2013) at Cape Verde. It is not obvious that this is true on global scale; we therefore also consider this production pathway. In this experiment CH_3I production is linearly coupled to light.

Opt134 Production from "normal" biological production and both photochemical production pathways: it is expected that in reality both biological and photochemical production occur simultaneously; we therefore include this experiment to represent combined production.

Opt24 Production from "stressed" biological production and photochemical production from refractory DOC: this combination of source processes was chosen as it became clear from Opt1–4, that "stressed" biological production and photochemical production from RDOC best represent observations in surface seawater on the global scale (see Sect. 3.1.2 and Table 3). The experiment considers "stressed" biological production with the ratio between CH_3I production and phytoplankton growth $k_{PP} \in [0.1232, 200]$ mmol CH_3I $(\text{kmolP})^{-1}$ and photochemical production from RDOC with the photochemical production rate $k_{photo} = 2.8 \times 10^{-7}$ m^2 mmol CH_3I $(\text{kmolP})^{-1}$ W^{-1} s^{-1}.

All rates for CH_3I production are identical to the ones used in Stemmler et al. (2013): no new parameter optimization was performed. For all experiments the ocean model was restarted from an 840 yr spin-up under preindustrial conditions, i.e. using a constant atmospheric CO_2 concentration of 278 ppm. A subsequent chemical spin-up run over 50 yr starting from a constant CH_3I concentration of 1 pmol L^{-1} was performed to ensure steady state conditions. The ocean model was forced with Ocean Model

BGD
10, 17549–17595, 2013

Intercomparison (OMIP) data (Röske, 2006). Model results presented here are from a one-year simulation that followed the spin-up.

2.3 Observations

CH_3I data are extracted from the HalOcAt database (https://halocat.geomar.de/, Ziska et al., 2013). HalOcAt was initiated in May 2009 as an initiative of SOLAS Project Integration as part of COST Action 735 (an EU-funded networking tool) and SOPRAN (http://sopran.pangaea.de/). Currently the data base contains about 200 datasets with a total of 55 400 oceanic and 476 000 atmospheric concentrations from all depth and height levels of 19 different halocarbon compounds (mainly very short-lived brominated and iodinated trace gases) from the years 1989 to 2011. Here only data from the upper 20 m of the ocean are used to evaluate the model performance (Fig. 1). Generally observed data from a particular month are compared to modelled monthly means. The exact origin of the individual data can be identified from the supplemental information (SI) in Ziska et al. (2013). Among other sources listed in Ziska et al. (2013), observations from air and seawater of the Atlantic are from Butler et al. (2007); Chuck et al. (2005); Jones et al. (2010); Schall et al. (1997); Wang et al. (2009), of the Pacific from Butler et al. (2007); Yokouchi et al. (2008), of the Southern Ocean from Abrahamsson et al. (2004); Butler et al. (2007); Chuck et al. (2005); Yokouchi et al. (2008), and of other ocean regions from Archer et al. (2007); Orlikowska and Schulz-Bull (2009); Yokouchi et al. (2008).

BGD
10, 17549–17595, 2013

3 Results

3.1 Global CH_3I production and distribution

3.1.1 Simulated mean fields

In the model biological methyl iodide production is proportional to primary production. Two experiments were performed, one with "normal" biological production, in which the ratio between CH_3I production and primary production is kept constant (Opt1), the other with a varying ratio (Opt2), which is high in oligotrophic oceans and low where plenty of nutrients are available. In total approximately 400 Gg of CH_3I are produced by phytoplankton within one year, but more than 94 % are lost via degradation and outgassing (Table 2).

In Opt1 spatial and temporal patterns of CH_3I production mirror the ones of primary production (Fig. 1a). Highest production throughout the year occurs in the equatorial upwelling, and seasonally in the Southern Ocean (in boreal fall and winter) or northern Pacific and Atlantic (in boreal spring and summer). Strong outgassing and degradation lead to a relatively short overall residence time τ ($\tau = \frac{\text{inventory}}{\text{sinks}}$) in the ocean of approx. 20 days. Consequently, in most oceanic regions CH_3I does not accumulate and the spatial patterns resemble the ones of primary production (Figs. 2a and 3a). In contrast, CH_3I concentrations in the Arctic Ocean are high in summer and fall despite low primary production (not shown). The reasons for this are small losses, i.e. reduced outgassing in summer when the wind speed is low and slow chemical reactions (hydrolysis, nucleophylic substitution) at cold temperatures.

In Opt2 the presence of stressed picocyanobacteria cells that lead to enhanced CH_3I production is simulated by implementing the ratio between CH_3I production and growth k_{PP} as a function of nutrient availability (Stemmler et al., 2013). This way k_{PP} is spatially and temporally variable with maxima in the subtropical gyres and minima in nutrient rich regions such as upwelling regimes (Fig. 3b). The inhomogeneous production rate leads to different CH_3I distribution patterns compared to primary production (Figs. 2b

BGD
10, 17549–17595, 2013

and 3a). Though concentration maxima at the Equator persist, more CH_3I is produced and remains in the subtropical gyres, whereas CH_3I in the Southern Ocean is reduced. These changes in the spatial distribution of CH_3I production go in line with changes in the relative importance of the loss processes and subsequently a different residence time. As production is reduced in the windy storm track regions of the Southern Hemisphere and intensified in the warmer subtropical regions the relative importance of outgassing is reduced compared to Opt1 (in the global budget, see Table 2), whereas the temperature- and light-dependent degradation processes gain in importance. The global oceanic residence time in this experiment is only 11 days (Table 2).

Photochemical production of CH_3I is parameterized as linearly coupled to the dissolved organic carbon (DOC) concentration and photosynthetically active radiation. Experiment Opt3 uses the DOC pool of HAMOCC (Fig. 5b). This semi-labile DOC (SLDOC) originates from exudation by plankton, is remineralized at a constant decay rate and is transported by advection and diffusion. Thus, high DOC concentrations are located in highly productive regions (Fig. 5b) and dispersion within its life time of a few months leads to dilution of the gradients that originate from primary production (compare Figs. 3a and 5b). The spatio-temporal patterns of CH_3I follow the ones of SLDOC and roughly resemble the ones in Opt1, but at generally lower concentrations (Fig. 4). Global production is much lower in this experiment (approx. 125 $Gg\,yr^{-1}$, Table 2), but due to the similar spatial distribution the residence time (approx. 17 days) is close to the one in Opt1.

In a second experiment on photochemical production, the DOC concentration used in the CH_3I source parameterization was kept constant instead of using the prognostic DOC tracer. This mimicks a "virtual" refractory DOC (RDOC) pool, i.e. an unlimited DOC supply. Here, the spatial distribution of CH_3I production is solely determined by incoming solar radiation (Fig. 5a). CH_3I concentrations are a function of the source strength relative to the sinks (degradation, outgassing). The CH_3I concentration distribution hence does not directly reflect SW radiation, but differs significantly from it (Fig. 4). For example in the tropical Pacific the CH_3I concentration is strongly influ-

BGD
10, 17549–17595, 2013

enced by the wind speed: in higher wind speed areas, like in the tropical easterlies north of the Equator (at 150° W westward) concentrations are lower than at low wind speed closer to the American coast due to enhanced outgassing. The residence time of 21 days is similar to the one in Opt1 and Opt3.

Two experiments were performed that consider more than one CH_3I production pathway: (1) Opt134, which includes "normal" biological production, and photochemical production by degradation of refractory and semi-labile DOC, (2) Opt24, which includes photochemical production by degradation of refractory DOC and biological production including enhanced production during stress. In Opt134 the methyl iodide is almost exclusively produced via the photochemical production pathway, less than 1 % is produced by phytoplankton (Fig. 7, Table 2). Thereby 72 % are produced via the unlimited DOC pool (RDOC), and 28 % from the semilabile DOC (Table 2). The spatial distribution (Fig. 6) is hence very similar to the one in Opt4 (Fig. 4). Differences occur where production from SLDOC is strongest, i.e. in the equatorial Pacific, in the Southern Ocean in boreal winter and in the North Pacific in boreal summer. There, concentrations are higher than in Opt4 due to higher production triggered by spatial DOC maxima (Fig. 5). The total CH_3I production in Opt134 is 60 % higher than in Opt4. But, the inventory is only ≈ 10 % higher as the additional production occurs in regions of high wind speed or temperature and is hence outgassing to the atmosphere (Fig. 11). The shift of the production towards warm and windy regions, which both support CH_3I loss, leads to a significant reduction of the global residence time in Opt134 (14 days) compared to Opt4 (21 days).

In Opt24 70 % of the methyl iodide is produced via the photochemical, and 30 % via the biological production pathway (Table 2). Biological production dominates only in the equatorial Pacific and Atlantic, in the Southern Ocean in boreal fall (September–November), and in the North Atlantic in spring and the Arctic in summer (boreal summer, not shown). Again, this implies that production is enhanced in regions where the life time of CH_3I is low as temperature and wind conditions favour degradation and outgassing. Yet not all of the freshly produced CH_3I is lost, and the concentrations at

BGD
10, 17549–17595, 2013

e.g the Equator are enhanced compared to Opt4. The global production of 306 Gg yr^{-1} is in between the ones of the single source experiments, Opt2 (407 Gg yr^{-1}) and Opt4 (217 Gg yr^{-1}).

3.1.2 Model evaluation

The simulated surface methyl iodide concentrations are compared with observations (Figs.1, 8, and S1–S25). Generally, the model represents methyl iodide observations well (see Supplemental information Fig. S1–S25), i.e. model predicted surface concentrations are in the order of magnitude of the observed ones in all experiments. Observed concentrations in the Atlantic span a wide range of < 0.1 pmol L^{-1} (Chuck et al., 2005) to 45 pmol L^{-1} (Smythe-Wright et al., 2006). But, values of higher 20 pmol L^{-1} are rare in the open ocean; typical concentrations are between 1 pmol L^{-1} and 15 pmol L^{-1} (Butler et al., 2007; Chuck et al., 2005; Jones et al., 2010; Schall et al., 1997; Wang et al., 2009) (see SI for individual cruise data). In contrast to other biogenic organohalogens, methyl iodide concentrations often do not show a pronounced maximum at the Equator. Ship cruise data covering a broad range of latitudes in the Atlantic in boreal fall (cruise Blast 2 October–November 1994 (Butler et al., 2007), Figs. 1, 8a and S1) reveal relatively homogeneous methyl iodide concentrations. Here, model experiments with biological CH_3I production (Opt1, Opt2) show an unrealistic maximum around the Equator, where nutrient upwelling, warm temperatures, and high insolation favour phytoplankton growth. The consideration of enhanced production by stressed picocyanobacteria (and not only "normal" biological production) significantly improved the representation of CH_3I along the ship track in the Atlantic. In Opt1 CH_3I concentrations show steep gradients between low concentrations in the oligotrophic subtropical gyres and high concentrations in the nutrient rich equatorial region. The consideration of a higher CH_3I production under nutrient shortage compensates for the low primary production and brings CH_3I concentrations closer to observations. It is only at the

BGD
10, 17549–17595, 2013

Equator where this experiment (Opt2) still overestimates observed concentrations by a moderate factor of approx. 1.3.

Though the experiments that consider solely photochemical production do not show a strong latitudinal gradient along the ship track neither, they tend to underestimate observed methyl iodide concentrations. But also observations are equivocal regarding that gradient: in contrast to Butler et al. (2007) (BLAST 2, Fig. S1) and Chuck et al. (2005) (Polarstern Cruise ANT XVII/1 September and October 2000, not shown), Tanzer and Heumann (1992) find an increase in CH_3I concentrations in the Atlantic towards the Equator on the same ship track (Polarstern Cruise ANT VII/5 in March and April 1989, not shown).

One similar feature is the east–west gradient in the subtropical North Atlantic in spring and summer (Figs. 8b and S10) in the biological experiments. This gradient evolves from low production in oligotrophic areas and higher production (and subsequent DOC formation) in more nutrient rich areas. Observations do not show this gradient, as concentrations in subtropical gyres are usually higher or as equally high as in other open ocean regions. This is improved in the experiments Opt2, Opt4 and the mixed source experiments.

For the Atlantic some information on the seasonal cycle of CH_3I concentrations is available from Wang et al. (2009). They find maxima in summer in the North East Atlantic south of Greenland (compare Figs. S21–S23). The model experiments Opt1 and Opt2 show maxima in spring, only the experiments that are dominated by photochemical production show maxima in summer, with a similar magnitude in and difference between the seasons as in the observations.

In the study of Bell et al. (2002) CH_3I production was simulated using the same parameterization as in our experiment Opt3. In Bell et al. (2002) CH_3I concentrations have been overestimated in Labrador seawater by 1–2 orders of magnitude compared to Moore and Groszko (1999) and Moore and Tokarczyk (1993). In experiment Opt3 concentrations in Labrador sewater are reduced, but this does not imply a model improvement, as spatial gradients elsewhere (e.g. in Subtropical gyres) are not repre-

BGD
10, 17549–17595, 2013

sented satisfactorily (see above). In the experiments Opt2 and Opt4 in contrast, concentrations in the Labrador Sea are improved compared to Bell et al. (2002) and spatial patterns on other ocean regions are similar to observed patterns. Both experiments show CH_3I concentrations of 2–7 pmol L^{-1} in July and hence are in the range of observed concentrations in the Labrador Sea (1–6 pmol L^{-1}, Moore and Groszko, 1999). This is achieved without implementation of an additional (biological) sink, which was suggested by Bell et al. (2002) to compensate for overestimations.

In the Pacific observed concentrations range between 0.3 and 12 pmol L^{-1} (Butler et al., 2007). There are less data for the western Pacific, and these reveal lower concentrations (often below 1 pmol L^{-1}) than in the eastern Pacific (3–12 pmol L^{-1}), though one has to note that the ship cruises are from different seasons. Model results also show lower values in boreal fall in the western Pacific, and higher values in the eastern Pacific. But, experiments with biological production of methyl iodide show partly strong (up to a factor of 5) overestimations of modelled concentrations in biologically productive areas, such as the tropical Pacific (Figs. 8c, d, S8, S11, and S13) or coastal upwelling areas (Fig. S9). HAMOCC is a state-of-the-art marine biogeochemical model, but certain aspects have to be considered that affect methyl iodide production. Biological production of CH_3I in the model is proportional to primary production that can not be evaluated easily on global scale. The biogeochemical model is tuned to capture main features of the nutrient (phosphate, nitrate, iron) distributions and simulate reasonably export production. Some features, like the large-scale distribution of primary production, are well represented, as primarily driven by nutrient supply and insolation. One known weakness in more or less all global models, is the so called “nutrient trapping” in the equatorial Pacific (summarized in Dietze and Loeptien, 2013), where too high nutrient concentrations at the surface lead to too high primary and export production in the equatorial Pacific. Hence deviations of modelled and observed CH_3I concentrations in the tropical Pacific (e.g. Fig. 8c) can not be unambiguously translated into the likeliness of a certain production pathway.

BGD
10, 17549–17595, 2013

In the Southern Ocean observations show both concentrations lower 5 pmol L^{-1} (e.g. west of 66° W in MAM Fig. 1) and values higher 5 pmol L^{-1} (30–90 ° E in MAM). The distinct seasonal cycle seen in many model experiments can not be extracted from observations, because the data coverage is sparse. Also a higher coverage might not show this feature clearly, because the concentration distribution is very variable in that region (see Figs. S14–S20).

To determine the production pathway(s) that dominate(s) surface concentrations for each location the experiment was identified that matches closest the observed value. This was done by first calculating the absolute deviation between simulated and observed concentrations for each observational data point and experiment. After ranking the experiments, the experiments that show the lowest deviation are mapped (Fig. 9) and the number of occasions when the deviation of a particular experiment was lowest was counted. Table 3 lists these numbers for each experiment relative to the total number of observations. As this is only a relative measure, three additional indicators are derived: the global root mean of the individual squared deviations, the global root median of the individual squared deviations (as they are not symmetrically distributed), and the median of the individual ratios of observations and simulated concentrations (to account for the spatial variability of concentrations).

First we start with the hypothesis that CH_3I is produced via one dominating source process, thus we only consider Opt1–4 in the analysis. At first, none of the ship cruises or seasons shows a concordant preference for one single experiment, but instead they show a mixture of various sources best representing certain locations without any obvious pattern (Fig. 9a). Testing if the deviation factor between modelled and observed concentrations is determined by some physical or biological mechanism did not reveal any systematic feature, e.g higher/lower deviations in regions with high/low primary production. This means that the underestimations in oligotrophic regions are equally high as e.g. overestimations in productive regions. On global scale, Opt4 (the experiment that mimics photochemical production from RDOC) is the most successful one among the single-source experiments, showing the lowest deviation for 46.27 % of the obser-

BGD
10, 17549–17595, 2013

vations, followed by Opt2, which represents 24.15 % of the observations best (Table 3). The difference of root mean and root median square deviations (Table 3) illustrates the pronounced skewness of the distribution of the squared deviations. Globally, the deviation of simulated and observed concentrations is lower for Opt4 compared to Opt1, Opt2, and Opt3. The second lowest deviation globally is found for experiment Opt3, in contrast to the second rank in the number of best matches found for Opt2. This simply reflects the spatial inhomogeneity of the deviations: whereas Opt2 is closer to the observations more often than Opt3, the deviations are higher in particular in the biologically productive equatorial upwelling. Opt3 furthermore underestimates observations more strongly than Opt4 and Opt2, indicated by the highest median ratio of observations and simulated concentration.

Next we consider the hypothesis that methyl iodide is always produced from mixed biological and photochemical sources, thus we consider only Opt24 and Opt134 in the analysis. The analysis of the number of "best matches" identifies Opt24 as the more successful experiment, being closest to approx. 60 % of the observations (Table 3). The root mean and root median squared deviations and the median ratio of observations and simulated concentrations show (Table 3), that actually both experiments represent observations equally well. This is no surprise, as in both experiments photochemical production is the dominant source (Fig. 7). This also explains why the mixed source experiments do not lead to significant improvements over the single source experiments. Of course, repeated parameter optimizations with different criteria, e.g weighting of deviations in biologically productive or upwelling regions stronger than other regions, may lead to a different source apportionment and may result concentrations distributions more different from the single source experiments. But, we refrain from conducting this, because it would not directly lead to new insights about the substances, but rather constitute a fine-tuning of the model.

In a last step we do not restrict the analysis towards the number or nature of CH_3I source processes, but take all experiments into account. The analysis of the number of lowest deviations reveals, that photochemical production from RDOC, i.e. Opt4, glob-

BGD
10, 17549–17595, 2013

ally explains the larges fraction of observations (34 %), followed by Opt134 (18 %) and Opt2 (16 %) . This is also reflected by the fact that Opt4 shows the lowest overall (i.e. global mean and median) deviation from observations.

3.2 Covariation of CH_3I with biotic and abiotic variables

Often covariation of proxy-parameters (such as temperature, radiation, or chlorophyll concentration) with measured methyl iodide concentrations are used to identify the dominant production pathway (e.g. Rasmussen et al., 1982; Happell and Wallace, 1996; Abrahamsson et al., 2004; Chuck et al., 2005; Wang et al., 2009; Lai et al., 2011). In the current study we know exactly from which production process the simulated methyl iodide originates, so we can test the robustness of some common predictors. For this purpose the correlations between simulated methyl iodide surface concentrations and simulated temperature (sst), phytoplankton concentration (phy), as well as solar radiation (rad) along an arbitrary track (the 30° W meridian 60° N–60° S) were derived for each month individually. For the CH_3I concentrations simulated in Opt1, the correlation with the phytoplankton concentration is indeed always stronger than the ones with temperature or radiation (Fig. 10). For Opt2 in contrast, in some month the correlation with radiation is strongest and no covariation with phytoplankton is observed (in September: $R(CH_3I, \text{phy}) < 0.1$ and $R(CH_3I, \text{rad}) = 0.79$). For Opt3 the covariation analysis along 30° W indicates in almost all months a strong relation with both phytoplankton and radiation (Fig. 10). Thereby the temporal pattern of the correlation coefficients follows the one of the correlation of the two parameters ($R(\text{phy}, \text{rad})$, Fig. 10d), and only when this correlation is low, e.g. in September and October, the correlation with temperature is highest. In Opt4, methyl iodide is co-varying with radiation and in all months CH_3I shows high, statistically significant, correlation coefficients (i.e. 0.6–0.9, Fig. 10). But, correlations with phytoplankton and temperature are also high, and often (in January, February, October, and December) even higher than correlations with radiation.

BGD
10, 17549–17595, 2013

From the source apportionment (Fig. 6) one expects for both experiments with mixed CH_3I sources similar correlation coefficients with temperature, phytoplankton and radiation as in Opt4, as photochemical production from a constant DOC pool is almost everywhere the dominant production pathway (apart from a small region around Equator in Opt24, where biological production is equally important, see Fig. 6b). As a matter of fact, the temporal pattern of the correlation coefficients is almost identical among Opt4, Opt134, and Opt24. When looking into individual months, in Opt24 always either the correlation with phytoplankton or the correlation with radiation is highest. Opt123 shows the same order in the correlation coefficients as Opt4, except in March.

3.3 Gas-exchange with the atmosphere

Air-sea exchange is analysed for the experiments that represent observed CH_3I concentrations best, Opt4, and for the ones with mixed CH_3I sources, Opt24 and Opt134.

As the prescribed atmospheric boundary conditions are identical in all experiments, differences among simulated saturation anomalies and gas fluxes are controlled only by differences of CH_3I dissolved in surface sea water. Air-sea fluxes can be both positive (into air) and negative (into the ocean), depending on season and location (Fig. 11). The seasonal mean emission ranges between −200 and 1500 $\mathrm{pmol\,m^{-2}\,h^{-1}}$. In line with highest concentrations, strongest outgassing is simulated in boreal winter in the Southern Ocean, where high production co-locates with high wind speeds. Note that the seasonal mean distributions shown in Fig. 11 suggest a strong spatial homogeneity, which in reality does not exist. At higher temporal resolution (e.g. daily means), the emissions are very "patchy", and the flux in neighboring regions in the Southern Ocean can differ by more than 1000 $\mathrm{pmol\,m^{-2}\,h^{-1}}$ (see SI Fig. S26 daily mean emissions over the first 120 days of the year). This inhomogeneity is caused by small scale low pressure systems that travel along the Southern Hemisphere storm track and lead to episodic high wind speeds. Furthermore, the daily mean data are characterised by a wider range of fluxes (−225 and 3687 $\mathrm{pmol\,m^{-2}\,h^{-1}}$), than the seasonal means (see above).

BGD
10, 17549–17595, 2013

In boreal summer, strong outgassing is found in the mid-latitude North Atlantic and North Pacific. Generally, lower emissions are predicted for the tropical and polar regions. This is due to weaker winds, that partly (e.g in Opt24 in the tropical Pacific) lead to low emissions, despite high production. In polar regions the sea ice cover seasonally shields the ocean from direct contact with the atmosphere and thereby suppresses outgassing. In all experiments a reversal of the air sea flux is predicted for the same region in boreal winter in the North Atlantic ($>50^{\circ}$ N).

Overall, global annual fluxes range between 100 and 170 $Gg\,yr^{-1}$ (Table 2), i.e. the ocean is a net source of methyl iodide for the atmosphere. Global emissions reported in the literature are often estimated from observed oceanic concentrations (and ideally simultaneously measured atmospheric concentrations), which are used to first calculate an emission flux, which is then extrapolated to the global scale (e.g Liss and Slater, 1974; Moore and Groszko, 1999; Smythe-Wright et al., 2006; Butler et al., 2007; Ziska et al., 2013). Global emissions simulated here are at the lower edge of these previously estimated values (Table 4). In general deviations can be due to both, uncertainties in the emission estimate and in the simulated fluxes, so all values listed in the table are discussed separately.

The global flux of 270 $Gg\,yr^{-1}$ reported in Liss and Slater (1974) is calculated from observations of CH_3I in the marine boundary layer of the Atlantic (approx. 60° N to 50° S) collected during a ship cruise in 1970–1971 (Lovelock et al., 1973). Unfortunately, only the mean values of atmospheric and oceanic volume mixing ratios are reported, together with the note that they did not find any obvious latitudinal trend, but large local variations. Our results also suggest an only weak latitudinal variation in the sea water concentration in fall (Fig. 1) across the Atlantic (Opt4, Opt134, Opt24), but a strong seasonal variation with concentrations lower ($<0.5\,pmol\,L^{-1}$) than the value reported in Lovelock et al. (1973). In particular our simulations suggest a reversal of the flux in the North Atlantic in winter. Altogether this can lead to deviations of the simulated global flux which is lower by approx 35–50 %.

BGD
10, 17549–17595, 2013

Rasmussen et al. (1982) aggregate 450 samples of atmospheric concentrations and much less ($21 + x$, not clearly phrased in their article) oceanic observations (which were not taken simultaneously) into fluxes for biologically unproductive, moderately productive and highly productive regions, which are assumed to hold a share of 60 %, 30 %, and 10 % of the ocean surface, respectively. Our results are to be compared to the sum of their unproductive and moderately productive ocean contributions, as highest production occurs in coastal regions (on shelves), for which this global model is not configured. The emission estimate is identical to the one by Liss and Slater (1974) and the deviation arises from the same causes, namely an under-representation of the seasonal variation of seawater concentrations and the simulated temporal reversal of gas exchange.

Singh et al. (1983) measured CH_3I in seawater and air on a ship cruise in November–December 1981 in the eastern Pacific, close to the American coast. The measured mean air concentration of 2 ppt is higher than the atmospheric concentrations used for modelling in that region (0.5–1.5 ppt, see Ziska et al., 2013). Simulated oceanic concentrations across that ship track range between 2.5–3.9 pmol L^{-1} in Opt4, and 3–35 pmol L^{-1} in Opt24, Opt134 and are comparable with the observed range of approx. 3–47 pmol L^{-1}. Hence, our simulated fluxes may be slightly higher here, despite comparable seawater concentrations, due to a stronger saturation anomaly. But, simulated concentrations (and fluxes) along that cruise track are higher than in other regions (see Fig. 9a, e, i and d, h, l) and thus the global flux is lower than the estimate by Singh et al. (1983).

Campos et al. (1996) measured CH_3I in the North Sea and report sea water concentrations of 3–14 pmol L^{-1} and estimate an average annual flux of 374.8 pmol m^{-2} h^{-1}. This value is close to the simulated values in the North Sea (though the model is not meant to reproduce conditions there) and at the same time close to the global mean value of simulated annual mean emissions (e.g. 385 pmol m^{-2} h^{-1} in Opt134). Hence, extrapolating the value found in the North Sea to a global CH_3I flux assuming a globally

BGD
10, 17549–17595, 2013

homogeneous distribution leads only by chance to a value similar to the simulated one, as the assumption is not valid.

The emission estimate presented by Moore and Groszko (1999) is based upon concentrations in air and water derived from three ship cruises in the Labrador and Sargasso Sea (July 1995), the Pacific from 47° N at the USA Coast to 47° S in Australia (Seattle–Hobart in October/November 1995), and the eastern Atlantic off Ireland (June 1996). Based on these measurements they calculate a CH_3I flux of 666.7 (75–2666.7) pmol m^{-2} h^{-1} for the Pacific, 495.8 (12.5–2292) pmol m^{-2} h^{-1} for the Labrador Sea and 1041 (12.5–4500) pmol m^{-2} h^{-1} for the eastern Atlantic. Using these values and an uncertainty analysis of the wind speed data they come up with a global range of approx. 130–350 Gg yr^{-1}. The derived local fluxes are in line with our simulated values and deviations between the global values are again caused by spatial and temporal variations.

Bell et al. (2002) calculate their emissions from a model simulation that uses the same parameterization of CH_3I production as in Opt3. As our simulated seawater concentrations are at many locations lower, our global CH_3I flux is consequently lower, despite similar air concentrations. Notably their model simulation does not predict a reversal of the gas exchange in the Northern Atlantic. Here our model predicts a seasonal mean of 0.2–0.3 ng L^{-1} in seawater which is lower than the value in Bell et al. (2002) (0.5 ng L^{-1}), and atmospheric concentrations in that particular region are mostly approx. 0.9 ppt (0.6–0.97 ppt), so slightly higher than their value of 0.6 ppt.

Smythe-Wright et al. (2006) report a mean CH_3I flux produced by *Prochlorococcus* from their ship cruise measurements of oceanic and atmospheric concentrations of 109.5 nmol m^{-1} d^{-1}. Based on this value and the ocean surface in the area of *Prochlorococcus* occurrence (in lower latitudes 40° S–40° N) they estimate a contribution of 610 Gg yr^{-1}. This result can be best compared to the values simulated in Opt2, the experiment that mimics *Prochlorococcus* and enhance production during stress, in which temporally, i.e. during strong nutrient limitation the production ratio k_{PP} is close to the one suggested in Smythe-Wright et al. (2006) (see Fig. 3b and Stemmler et al.,

BGD
10, 17549–17595, 2013

2013). As the maximum concentrations in Opt2 are lower than the observed maximum of 40 pmol L^{-1}, and as Smythe-Wright et al. (2006) assume that these high values prevail all year long, whereas the model simulation resolves an intra-annual variation, our estimate of the contribution of this source is much lower, namely only 173 Gg yr^{-1}. Even the global emissions, i.e. including regions where the biological CH_3I source can not be attributed to picocyanobateria, are much lower than their value (218.6 Gg yr^{-1} Table 2). The increase of the global emission versus the regional emission is only small, because the majority of the flux is within 40° N and 40° S.

The global emission estimates by Butler et al. (2007) are based on observed CH_3I from seven ship cruises from 1994–2004 covering all seasons. They cluster the results into fluxes of four types, "Tropics", "Southern Ocean", "Gyres", and "Coastal waters". The measured atmospheric concentrations are consistent with the ones used in this study. They calculate mean fluxes of 542 pmol m^{-2} h^{-1} for the "Tropics", 708 pmol m^{-2} h^{-1} for the "Southern Ocean", and 583 pmol m^{-2} h^{-1} for the "Gyres". These values are comparable to the simulated fluxes, though the regional distribution (i.e. ratio between the defined clusters) is different for different experiments, and shows a clear seasonality. Also here their global estimate for the open ocean is lower than our simulated value due to the seasonal and spatial variability. In detail, e.g. their value for the Southern Ocean is determined from ship cruises in November–December 2001, and February–April 1996. Our simulation suggests that concentrations and fluxes are higher in these months than in the Southern Hemisphere winter season. They furthermore do not cover the winter season in the region where the model predicts subsaturation of the ocean by CH_3I. Thus it is consistent, that our simulated global values are lower than the estimates in Butler et al. (2007).

Jones et al. (2010) estimate regional emissions from the oligotrophic and mesotrophic open ocean, shelf, coastal, and upwelling regions from simultaneous measurements of seawater and air concentrations during two ship cruises in the North Atlantic in June–July 2006 (shelf, coastal, and upwelling are not listed in Table 4). Their mean seawater concentrations in the oligotrophic ocean are 6 pmol L^{-1}, whereas the

BGD
10, 17549–17595, 2013

model predicts approx. 3 pmol L^{-1}. In the open ocean between 15–25° N they find on average 16 pmol L^{-1}, while our model predicts 1–4 pmol L^{-1}. Also concentrations in the open Atlantic 53–58° N are often higher in the observations (10.5, 3–21 pmol L^{-1}) than predicted values (6–9 pmol L^{-1}). Though the simulated values are in the range of observations, they are at the lower edge, therefore simulated fluxes are lower than the one derived by Jones et al. (2010).

As the emissions calculated in Ziska et al. (2013) are based on observed atmospheric and oceanic CH_3I concentrations, and our simulations predict concentrations that are close to the observed values and uses observed atmospheric concentrations as the upper boundary conditions, the global emissions are similar (Table 4). Differences occur in particular where gaps in the observations where filled by an interpolation method. For instance, in the central to western Pacific Ocean (approx. 10–40° S, 90–180° W), where no observational seawater concentrations were available, a local maximum is predicted, which is not reflected in our model; in contrast here a local minimum is simulated. Also in the Indian Ocean the emissions calculated by Ziska et al. (2013) rely solely on the extrapolation method. Here, their climatological flux is characterized by a distinct north–south gradient, with high values in the south. Though the gradient in their estimate by construction arises from remote observations, it is supported by the model simulations which also often predict a similar north–south gradient. In the climatology by Ziska et al. (2013) polar regions and the tropics are mostly in equilibrium, this is also the case in Opt4. Another prominent feature of their flux distribution pattern is the difference between the east and west Pacific in the lower latitudes (approx 35° S–35° N) characterised by high values in the east and low values in the west. This is partly also seen in model results, e.g. in boreal winter in Opt134, though with differences in the exact location of maxima in the east Pacific (see above).

One feature that is simulated, but not considered in most global estimates (apart from Ziska et al., 2013), is the reversal of the gas exchange. It is unclear whether the ocean can act as a sink for methyl iodide in certain locations and seasons. As the model uses temporally constant atmospheric boundary conditions based on observa-

BGD
10, 17549–17595, 2013

tions with gaps filled by interpolation (Ziska et al., 2013) and these observations in that region are particularly sparse, the robustness of the feature is uncertain. But, negative saturation anomalies in cold low light waters in the Greenland/Norwegian Sea were reported by Happell and Wallace (1996). They measured a mean atmospheric concentration of 2.4 pmol mol^{-1}, which is more than double the value we use in our simulations. Therefore we believe that the reversal is indeed a feature of low production, rather than caused by overestimated air concentrations.

To sum up, simulated fluxes are consistent with fluxes calculated from observed concentrations in the marine boundary layer. Deviations of our calculated global emission and the estimates derived from extrapolating local fluxes to the global scale are minor considering spatial and temporal variability of the fluxes.

4 Discussion and conclusions

In this study we show simulated global distribution patterns of CH_3I and air–sea fluxes. Different production pathways of CH_3I, i.e. biological and photochemical production mechanisms are considered. This is the first study since Bell et al. (2002) that assesses marine emissions of CH_3I based on process parameterizations of its sources and sinks in the open ocean. The evaluation of all model experiments with an available global observational data set (Ziska et al., 2013) reveals that best agreement is achieved when photochemical from refractory DOC or both photochemical and direct biological production are considered. Specifically, the highest proportion is due to production through photochemical degradation of refractory detritus (70 %); biological production by picocyanobacteria including enhanced production during stress accounts for the remaining part (30 %). This pathway has been proposed by Hughes et al. (2011) based on laboratory experiments.

Our findings shed some light on the source mechanisms of CH_3I. Previous model studies (Bell et al., 2002) and field observations (e.g. Happell and Wallace, 1996; Chuck et al., 2005; Smythe-Wright et al., 2006; Wang et al., 2009) have suggested

BGD
10, 17549–17595, 2013

either a photochemical or a biological source of CH_3I. In a recent model study, Stemmler et al. (2013) have shown that observed vertical CH_3I profile in the tropical East Atlantic can be best explained by biological production. The model results obtained do not contradict all these previous findings. Including only the photochemical pathway reflects the observed distribution patterns reasonably well, if the availability of methyl groups is not limiting the process. However, depending on the region or season photochemical or biological production may dominate. For instance, in the Southern Ocean the model suggests that biological production is dominant only in austral spring while in the equatorial Pacific CH_3I is biologically produced all year round. Thus, it is not surprising that correlations between methyl iodide and biotic or abiotic factors are not robust indicators to determine the source of CH_3I. The experiment where e.g. only the photochemical pathway is considered gives an equally high correlation coefficient of CH_3I with irradiance and phytoplankton and in certain months with low irradiance the correlation coefficient is even higher with phytoplankton. This is in line with Abrahamsson et al. (2004); based on observations they conclude that Chl *a* is not an adequate proxy for the production of organic halogens.

Despite the generally good agreement between model and observations, there are still some uncertainties that are related to regions where data are sparse (e.g. the Indian Ocean) or where seasonal variability is strong and the temporal resolution of observational data is insufficient (e.g. in the Southern Ocean). This is particularly crucial if the goal is to quantify emissions of methyl iodide. Our model results show that globally a net flux of methyl iodide from the ocean into the atmosphere takes place. However, on local scale the ocean can act both as a source and a sink of methyl iodide to the atmosphere. A flux from the atmosphere in the ocean takes place during the winter months at high latitudes of the North Atlantic Ocean. This seems to be a robust feature, because in all model experiment there is a net uptake of CH_3I by the ocean regardless of the production pathway. So far there are no observations that support or contradict this finding. Thus, we strongly suggest to perform measurements in this region to test the model's performance. A weakness of our current approach is the as-

BGD
10, 17549–17595, 2013

sumption of constant atmospheric concentrations that are used for the upper boundary condition. At least in high latitudes strong seasonal variability can be expected. Using a coupled ocean-atmosphere model would account for this temporal variability.

Overall we find significant differences in the emissions among the different model experiments. Thus, the production pathway is important to quantify the air–sea fluxes. Despite regional and temporal variability in the dominance of source mechanisms, global methyl iodide concentration can be reasonably well represented by time-averaged surface short-wave radiation patterns.

Supplementary material related to this article is available online at http://www.biogeosciences-discuss.net/10/17549/2013/bgd-10-17549-2013-supplement.pdf.

Acknowledgements. The authors are grateful to F. Ziska (Geomar, Helmholtz Centre for Ocean Research Kiel) for providing observational data and for valuable discussions. We thank K. Six (Max Planck Institute for Meteorology, Hamburg) for internal review of the manuscript. Model simulations have been performed with the IBM Power 6 supercomputer at the DKRZ (German Climate Computing Center). The study was funded by the German BMBF project SOPRAN (Surface Ocean Processes in the Anthropocene) SOPRAN 03F0662E.; IH is financed through the Cluster of Excellence "CliSAP" (EXC177), University of Hamburg, funded through the German Science Foundation (DFG).

Our colleague Ernst Maier-Reimer died during the finalization of this manuscript. He annotated an earlier version but had no chance to comment the latest one. We hope that he would approve of the changes we made.

References

Abrahamsson, K., Bertilsson, S., Chierici, S., Fransson, A., Froneman, P., Lorén, A., and Pakhomov, E.: Variations of biochemical parameters alonga transect in the Southern Ocean, with

BGD
10, 17549–17595, 2013

special emphasis on volatile halogenated organic compounds, Deep-Sea Res. Pt. II, 51, 2745–2756, 2004. 17551, 17556, 17565, 17573
Amachi, S.: Microbial contribution to global iodine cycling: volatilization, accumulation, reduction, oxidation, and sorption of iodine, Microbes Environ., 23, 269–276, 2008. 17551
Amachi, S., Kamagata, Y., Kanagawa, T., and Muramatsu, Y.: Bacteria mediate methylation of iodine in marine and terrestrial environments, Appl. Environ. Microb., 67, 2718–2722, 2001. 17551
Archer, S., Goldson, L., Liddicoat, M., Cummings, D., and Nightingale, P.: Marked seasonality in the concentrations and sea-to-air flux of volatile iodocarbon compounds in the western English Channel, J. Geophys. Res.-Oceans, 112, C08009, doi:10.1029/2006JC003963, 2007. 17556
Bell, N., Hsu, L., Jacob, D., Schultz, M., Blake, D., Butler, J., King, D., Lobert, J., and Maier-Reimer, E.: Methyl iodide: atmospheric budget and use as a tracer of marine convection in global models, J. Geophys. Res., 107, 8-1–8-12, 2002. 17551, 17552, 17554, 17561, 17562, 17569, 17572, 17584
Brownell, D., Moore, R., and Cullen, J.: Production of methyl halides by *Prochlorococcus* and *Synechococcus*, Global Biogeochem. Cy., 24, GB2002, doi:10.1029/2009GB003671, 2010. 17551
Butler, J., King, D., Lobert, J., Montzka, S., Yvon-Lewis, S., Hall, B., Warwick, N., Mondell, D., Aydin, M., and Elkins, J.: Oceanic distributions and emissions of short-lived halocarbons, Global Biogeochem. Cy., 21, GB1023, doi:10.1029/2006GB002732, 2007. 17550, 17551, 17556, 17560, 17561, 17562, 17567, 17570, 17584, 17592
Campos, M., Nightingale, P., and Jickells, T.: A comparison of methyl iodide emissions from sea water and wet depositional fluxes of iodine over the southern North Sea, Tellus B, 48, 106–114, 1996. 17568, 17584
Carpenter, L.: Iodine in the Marine Boundary Layer, Chem. Rev., 103, 4953–4962, 2003. 17550, 17551
Carpenter, L., Malin, G., Liss, P., and Küpper, F.: Novel biogenic iodine-containing trihalomethanes and other short-lived halocarbons in the coastal East Atlantic, Global Biogeochem. Cy., 14, 1191–1204, 2000. 17551
Chameides, W. and Davis, D.: Iodine: its possible role in tropospheric photochemistry, J. Geophys. Res., 85, 7383–7398, 1980. 17550

BGD
10, 17549–17595, 2013

Chuck, A., Turner, S., and Liss, P.: Oceanic distributions and air–sea fluxes of biogenic halocarbons in the open ocean, J. Geophys. Res.-Oceans, 110, 1–12, 2005. 17550, 17551, 17556, 17560, 17561, 17565, 17572

Dietze, H. and Loeptien, U.: Revisiting "nutrient trapping" in global coupled biogeochemical ocean circulation models, Global Biogeochem. Cy., 27, 265–284, doi:10.1002/gbc.20029, 2013. 17562

Elliott, S. and Rowland, F.: Nucleophilic substitution rates and solubilities for methyl halides in seawater, Geophys. Res. Lett., 20, 1043–1046, 1993. 17553

Elliot, S. and Rowland, F.: Methyl halide hydrolysis rates in natural waters, J. Atmos. Chem., 20, 229–236, 1995. 17553

Fuhlbrügge, S., Krüger, K., Quack, B., Atlas, E., Hepach, H., and Ziska, F.: Impact of the marine atmospheric boundary layer conditions on VSLS abundances in the eastern tropical and subtropical North Atlantic Ocean, Atmos. Chem. Phys., 13, 6345–6357, doi:10.5194/acp-13-6345-2013, 2013. 17550

Fuse, H., Inoue, H., Murakami, K., Takimura, O., and Yamaoka, Y.: Production of free and organic iodine by *Roseovarius* spp., FEMS Microbiol. Lett., 229, 189–194, 2003. 17551

Giese, B., Laturnus, F., Adams, F. C., and Wiencke, C.: Release of volatile iodinated C_1–C_4 hydrocarbons by marine macroalgae from various climate zones, Environ. Sci. Technol., 33, 2432–2439, doi:10.1021/es980731n, 1999. 17551

Gschwend, P., MacFarlane, J., and Newman, K.: Volatile halogenated organic compounds released to seawater from temperate marine macroalgae, Science, 227, 1033–1035, 1985. 17551

Happell, J. and Wallace, D.: Methyl iodide in the Greenland/Norwegian Seas and the tropical Atlantic Ocean: evidence for photochemical production, Geophys. Res. Lett., 23, 2105–2108, 1996. 17550, 17551, 17565, 17572

Hughes, C., Malin, G., Nightingale, P., and Lisa, P.: The effect of light stress on the release of volatile iodocarbons by three species of marine microalgae, Limnol. Oceanogr., 51, 2849–2854, 2006. 17551

Hughes, C., Malin, G., Turley, C., Keely, B., Nightingale, P., and Liss, P.: The production of volatile iodocarbons by biogenic marine aggregates, Limnol. Oceanogr., 53, 867–872, 2008. 17551

BGD
10, 17549–17595, 2013

Hughes, C., Franklin, D., and Malin, G.: Iodomethane production by two important marine cyanobacteria: *Prochlorococcus marinus* (CCMP 2389) and *Synechococcus* sp. (CCMP 2370), Mar. Chem., 125, 19–25, 2011. 17554, 17572

Ilyina, T., Six, K. D., Segschneider, J., Maier-Reimer, E., Li, H., and Núñez-Riboni, I.: Global ocean biogeochemistry model HAMOCC: model architecture and performance as component of the MPI-Earth system model in different CMIP5 experimental realizations, J. Adv. Model. Earth Syst., 5, 287–315, doi:10.1029/2012MS000178, 2013. 17552, 17553

Itoh, N., Tsujita, M., Ando, T., Hisatomi, G., and Higashi, T.: Formation and emission of monohalomethanes from marine algae, Phytochemistry, 45, 67–73, 1997. 17551

Jones, C., Hornsby, K., Sommariva, R., Dunk, R., Von Glasow, R., McFiggans, G., and Carpenter, L.: Quantifying the contribution of marine organic gases to atmospheric iodine, Geophys. Res. Lett., 37, L18804, doi:10.1029/2010GL043990, 2010. 17551, 17556, 17560, 17570, 17571, 17584

Karlsson, A., Auer, N., Schulz-Bull, D., and Abrahamsson, K.: Cyanobacterial blooms in the Baltic – a source of halocarbons, Mar. Chem., 110, 129–139, 2008. 17551

Lai, S., Williams, J., Arnold, S., Atlas, E., Gebhardt, S., and Hoffmann, T.: Iodine containing species in the remote marine boundary layer: a link to oceanic phytoplankton, Geophys. Res. Lett., 38, L20801, doi:10.1029/2011GL049035, 2011. 17551, 17565

Liss, P. and Slater, P.: Fluss of gas aceross the air–sea interface, Nature, 247, 181–184, 1974. 17567, 17568, 17584

Lovelock, J., Maggs, R., and Wade, R.: Halogenated hydrocarbons in and over the Atlantic, Nature, 241, 194–196, 1973. 17567

Manley, S.: The possible involvement of methylcobalamin in the production of methyl iodide in the marine environment, Mar. Chem., 46, 361–369, 1994. 17551

Manley, S. and Dastoor, M.: Methyl iodide (CH_3I) production by kelp and associated microbes, Mar. Biol., 98, 477–482, 1988. 17551

Manley, S. and De La Cuesta, J.: Methyl iodide production from marine phytoplankton cultures, Limnol. Oceanogr., 42, 142–147, 1997. 17551

Marsland, S., Haak, H., Jungclaus, J., Latif, M., and Röske, F.: The Max-Planck-Institute global ocean/sea ice model with orthogonal curvilinear coordinates, Ocean Model., 5, 91–127, 2003. 17552, 17553

BGD
10, 17549–17595, 2013

Moore, R. and Groszko, W.: Methyl iodide distribution in the ocean and fluxes to the atmosphere, J. Geophys. Res.-Oceans, 104, 11163–11171, doi:10.1029/1998JC900073, 1999. 17551, 17553, 17561, 17562, 17567, 17569, 17584
Moore, R. and Tokarczyk, R.: Volatile biogenic halocarbons in the northwest Atlantic, Global Biogeochem. Cy., 7, 195–210, 1993. 17551, 17561
Moore, R. and Zafiriou, O.: Photochemical production of methyl iodide in seawater, J. Geophys. Res., 99, 16415–16420, 1994. 17551
Nightingale, P., Malin, G., and Liss, P.: Production of chloroform and other low-molecular-weight halocarbons by some species of macroalgae, Limnol. Oceanogr., 40, 680–689, 1995. 17551
Nightingale, P. D., Malin, G., Law, C., Watson, A., Liss, P., Liddicoat, M., Boutin, J., and Upstill-Goddard, R.: In situ evaluation of airsea gas exchange parameterizations using novel conservative and volatile tracers, Global Biogeochem. Cy., 14, 373–387, 2000. 17553
Orlikowska, A. and Schulz-Bull, D.: Seasonal variations of volatile organic compounds in the coastal Baltic Sea, Environ. Chem., 6, 495–507, 2009. 17556
Rasmussen, R., Khalil, M., Gunawardena, R., and Hoyt, S.: Atmospheric methyl iodide (CH_3I) (Oregon), J. Geophys. Res., 87, 3086–3090, 1982. 17551, 17565, 17568, 17584
Rattigan, O., Shallcross, D., and Cox, R.: UV absorption cross-sections and atmospheric photolysis rates of CF3I, CH3I, C2H5I and CH2ICl, J. Chem. Soc. Faraday T., 93, 2839–2846, 1997. 17550, 17553
Richter, U. and Wallace, D.: Production of methyl iodide in the tropical Atlantic Ocean, Geophys. Res. Lett., 31, 1–4, 2004. 17551, 17552
Röske, F.: A global heat and freshwater forcing dataset for ocean models, Ocean Model., 11, 235–297, 2006. 17556
Schall, C., Heumann, K., and Kirst, G.: Biogenic volatile organoiodine and organobromine hydrocarbons in the Atlantic Ocean from 42° N to 72° S, Fresen. J. Anal. Chem., 359, 298–305, 1997. 17556, 17560
Singh, H., Salas, L., and Stiles, R.: Methyl halides in and over the eastern Pacific (40° N–32° S), J. Geophys. Res., 88, 3684–3690, 1983. 17550, 17568, 17584
Six, K. and Maier-Reimer, E.: Effects of plankton dynamics on seasonal carbon fluxes in an ocean general circulation model, Global Biogeochem. Cy., 10, 559–583, 1996. 17553
Smythe-Wright, D., Boswell, S., Breithaupt, P., Davidson, R., Dimmer, C., and Eiras Diaz, L.: Methyl iodide production in the ocean: implications for climate change, Global Biogeochem.

BGD
10, 17549–17595, 2013

Cyc., 20, GB3003, doi:10.1029/2005GB002642, 2006. 17550, 17551, 17560, 17567, 17569, 17570, 17572, 17584
Solomon, S., Garcia, R., and Ravishankara, A.: On the role of iodine in ozone depletion, J. Geophys. Res., 99, 20491–20499, 1994. 17550
Stemmler, I., Rothe, M., Hense, I., and Hepach, H.: Numerical modelling of methyl iodide in the eastern tropical Atlantic, Biogeosciences, 10, 4211–4225, doi:10.5194/bg-10-4211-2013, 2013. 17552, 17553, 17554, 17555, 17557, 17569, 17573, 17581
Tanzer, D. and Heumann, K.: Gas chromatographic trace-level determination of volatile organic sulfides and selenides and of methyl iodide in atlantic surface water, Int. J. Environ. An. Ch., 48, 17–31, 1992. 17561
Toda, H. and Itoh, N.: Isolation and characterization of a gene encoding a S-adenosyl-L-methionine-dependent halide/thiol methyltransferase (HTMT) from the marine diatom Phaeodactylum tricornutum: biogenic mechanism of CH_3I emissions in oceans, Phytochemistry, 72, 337–343, doi:10.1016/j.phytochem.2010.12.003, 2011. 17551
Vogt, R., Sander, R., Von Glasow, R., and Crutzen, P.: Iodine chemistry and its role in halogen activation and ozone loss in the marine boundary layer: a model study, J. Atmos. Chem., 32, 375–395, 1999. 17550
Wang, L., Moore, R., and Cullen, J.: Methyl iodide in the NW Atlantic: spatial and seasonal variation, J. Geophys. Res.-Oceans, 114, C07007, doi:10.1029/2007JC004626, 2009. 17551, 17556, 17560, 17561, 17565, 17572
Williams, J., Gros, V., Atlas, E., Maciejczyk, K., Batsaikhan, A., Schöler, H., Forster, C., Quack, B., Yassaa, N., Sander, R., and Van Dingenen, R.: Possible evidence for a connection between methyl iodide emissions and saharan dust, J. Geophys. Res.-Atmos., 112, D07302, doi:10.1029/2005JD006702, 2007. 17551
Yokouchi, Y., Nojiri, Y., Barrie, L., Toom-Sauntry, D., and Fujinuma, Y.: Atmospheric methyl iodide: high correlation with surface seawater temperature and its implications on the sea-to-air flux, J. Geophys. Res.-Atmos., 106, 12661–12668, 2001. 17551
Yokouchi, Y., Osada, K., Wada, M., Hasebe, F., Agama, M., Murakami, R., Mukai, H., Nojiri, Y., Inuzuka, Y., Toom-Sauntry, D., and Fraser, P.: Global distribution and seasonal concentration change of methyl iodide in the atmosphere, J. Geophys. Res.-Atmos., 113, D18311, doi:10.1029/2008JD009861, 2008. 17556
Youn, D., Patten, K. O., Wuebbles, D. J., Lee, H., and So, C.-W.: Potential impact of iodinated replacement compounds CF_3I and CH_3I on atmospheric ozone: a three-dimensional mod-

BGD
10, 17549–17595, 2013

eling study, Atmos. Chem. Phys., 10, 10129–10144, doi:10.5194/acp-10-10129-2010, 2010. 17551, 17552

Ziska, F., Quack, B., Abrahamsson, K., Archer, S. D., Atlas, E., Bell, T., Butler, J. H., Carpenter, L. J., Jones, C. E., Harris, N. R. P., Hepach, H., Heumann, K. G., Hughes, C., Kuss, J., Krüger, K., Liss, P., Moore, R. M., Orlikowska, A., Raimund, S., Reeves, C. E., Reifenhäuser, W., Robinson, A. D., Schall, C., Tanhua, T., Tegtmeier, S., Turner, S., Wang, L., Wallace, D., Williams, J., Yamamoto, H., Yvon-Lewis, S., and Yokouchi, Y.: Global sea-to-air flux climatology for bromoform, dibromomethane and methyl iodide, Atmos. Chem. Phys., 13, 8915–8934, doi:10.5194/acp-13-8915-2013, 2013. 17551, 17552, 17556, 17567, 17568, 17571, 17572, 17584

BGD
10, 17549–17595, 2013

Table 1. Model experiments, defined by production pathway considered. Experiments are called "Opt" to be consistent with Stemmler et al. (2013), who derived the CH_3I production rates from a parameter optimization.

Production pathway/ Experiment ID	biological		photochemical		mixed	
	Opt1	Opt2	Opt3	Opt4	Opt134	Opt24
"Normal" biological prod.	+				+	
"Stressed" biological prod.		+				+
Photochemical prod. from SLDOC			+		+	
Photochemical prod. from RDOC				+	+	+

BGD
10, 17549–17595, 2013

Table 2. Global production, loss, emission, and inventory.

Production pathway	biological		photochemical		mixed	
	Opt1	Opt2	Opt3	Opt4	Opt134	Opt24
Production [Gg yr^{-1}]	427.23	407.49	125.49	217.14	348.27	305.97
% biological	100	100			0.2	29
% photochemical SLDOC			100		28	
% photochemical RDOC				100	72	71
Net emission [Gg yr^{-1}]	256.62	218.55	69.09	101.52	170.61	149.46
Loss [Gg yr^{-1}]	141.00	180.48	53.58	109.98	164.97	148.05
Inventory [Gg]	22.56	12.69	5.64	12.69	14.10	11.28

BGD
10, 17549–17595, 2013

Table 3. Global fraction of observations best presented by the respective model experiment (as shown in Fig. 9 for individual locations and seasons), considering only single source experiments, only mixed sources experiments, and all experiments (upper part). Global root-mean-square deviation (RMSD, [pmol L^{-1}]), root-median-square deviation (RMSD(median), [pmol L^{-1}]), and global median of the ratio $\frac{\text{observation}}{\text{model}}$ (lower part).

Production pathway	biological		photochemical		mixed	
	Opt1	Opt2	Opt3	Opt4	Opt134	Opt24
Single source	13.12 %	24.15 %	16.46 %	46.27 %		
Mixed sources					39.31 %	60.69 %
All	7.63 %	16.56 %	12.14 %	34.27 %	18.17 %	11.23 %
Global RMSD [pmol L^{-1}]	7.78	10.11	2.97	2.63	3.14	3.21
Global RMSD (median) [pmol L^{-1}]	1.04	0.65	0.50	0.35	0.60	0.52
Median ratio $\frac{\text{observation}}{\text{model}}$	2.14	1.74	3.42	2.01	1.24	1.49

BGD
10, 17549–17595, 2013

Table 4. Global annual methyl iodide emissions [Gg yr^{-1}] from the ocean.

Source type	Lit. value	This study	Reference
Open ocean		101.52–170.6	Opt4,Opt134
Open ocean	270		Liss and Slater (1974)
"Unproductive" ocean	50		Rasmussen et al. (1982)
"Moderately productive" ocean	220		Rasmussen et al. (1982)
"Highly productive" ocean	1000		Rasmussen et al. (1982)
Open ocean	300–500		Singh et al. (1983)
Global ocean	150		Campos et al. (1996)
Global ocean	130–350		Moore and Groszko (1999)
Open ocean	214		Bell et al. (2002)
Open ocean 40° N–40° S	610	174 (219*)	Smythe-Wright et al. (2006), Opt2
Open ocean	298.1		Butler et al. (2007)
Global ocean	610.4		Butler et al. (2007)
Oligotrophic open ocean	138.6		Jones et al. (2010)
Mesotrophic open ocean	133.5		Jones et al. (2010)
Global ocean	205.8		Ziska et al. (2013) (OLS)
Global ocean	176.0		Ziska et al. (2013) (RF)

* Global value.

BGD
10, 17549–17595, 2013

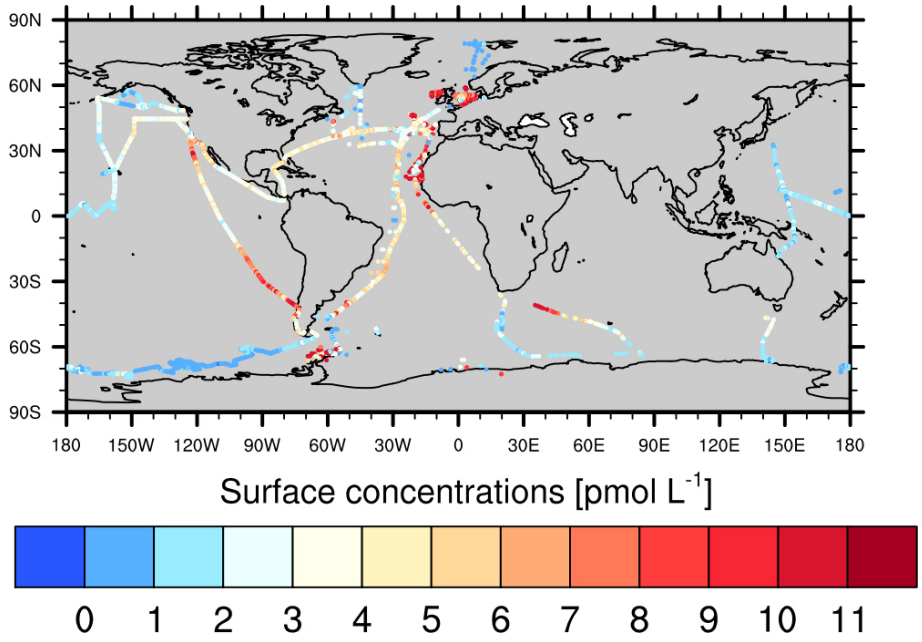

Fig. 1. Observed surface methyl iodide concentration [pmol L^{-1}].

BGD
10, 17549–17595, 2013

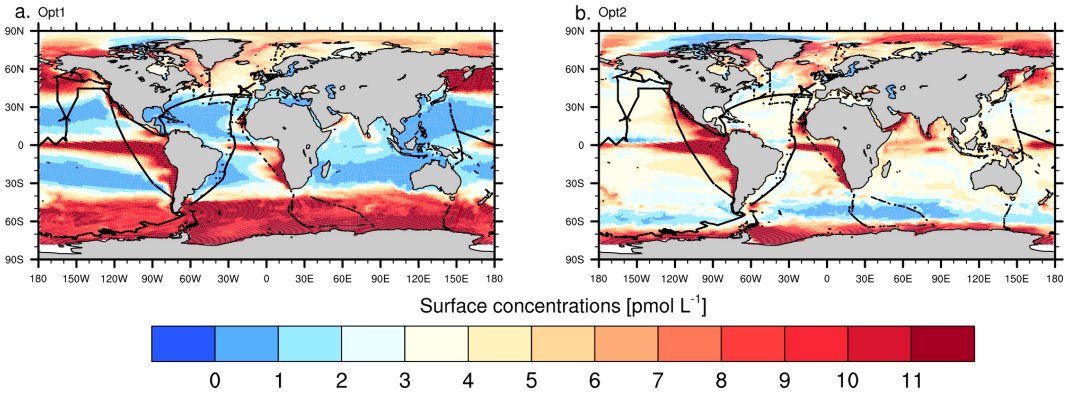

Fig. 2. Annual mean methyl iodide concentration [pmol L^{-1}] in the experiment with normal biological production, Opt1, **(a)** and with production from stressed picocyanobacteria, Opt2 **(b)**. Black dots mark sampling locations of CH_3I observations (shown in Fig. 1).

BGD
10, 17549–17595, 2013

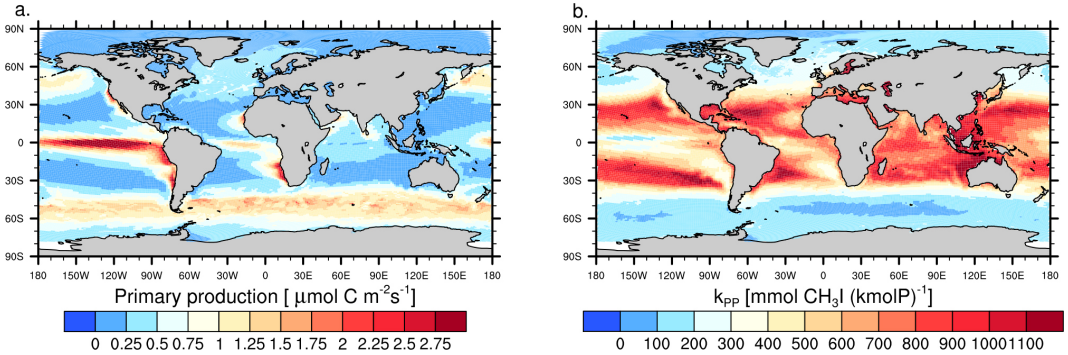

Fig. 3. Integrated annual mean primary production [$\mu mol\, m^{-2}\, s^{-1}$] **(a)** and mean ratio between methyl iodide and primary production rate k_{PP} [$mmol\, CH_3I\, (kmolP)^{-1}$] **(b)**.

BGD
10, 17549–17595, 2013

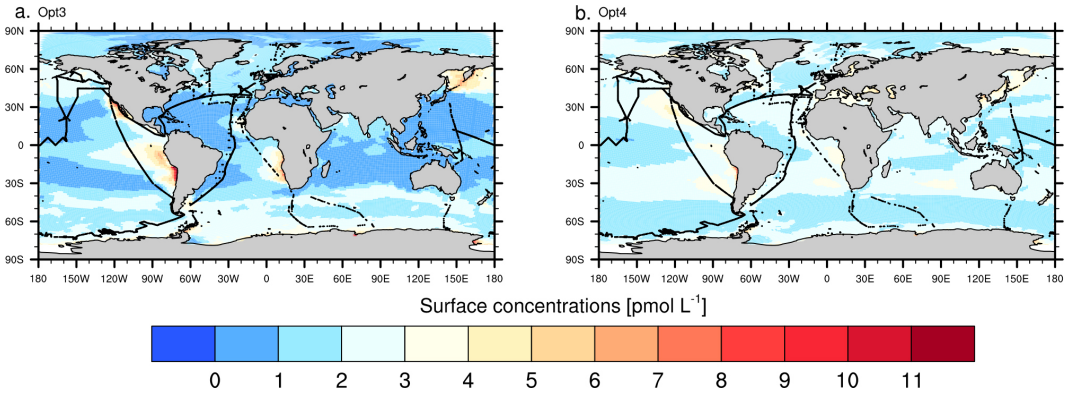

Fig. 4. Annual mean methyl iodide concentration [pmol L^{-1}] in the experiment with photochemical production from SLDOC, Opt3, **(a)** and RDOC, Opt4, **(b)**. Black dots mark sampling locations of CH_3I observations (shown in Fig. 1).

BGD
10, 17549–17595, 2013

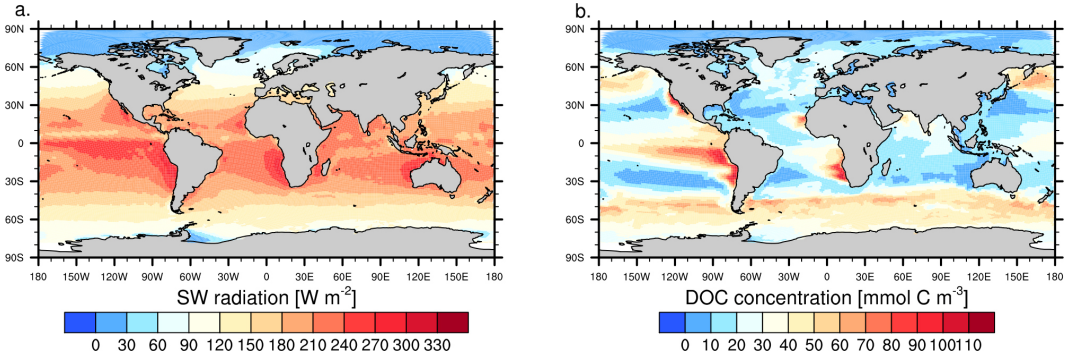

Fig. 5. Annual mean short-wave radiation [$W m^{-2}$] **(a)** and semi-labile DOC concentration [$mm C m^{-3}$] **(b)**.

BGD
10, 17549–17595, 2013

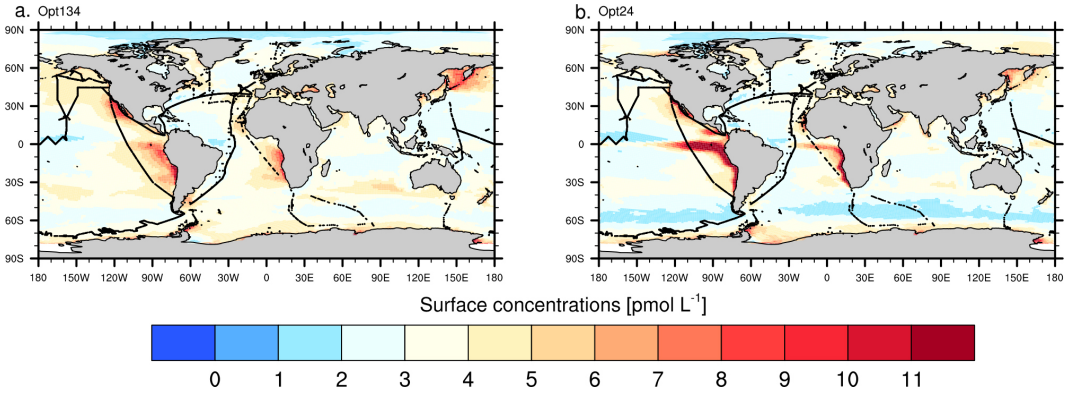

Fig. 6. Methyl iodide concentration [pmol L^{-1}] in the experiment with mixed biological and photochemical production, Opt134, **(a)** and the one with mixed biological production considering stressed picocyanobacteria and photochemical production from RDOC, Opt24, **(b)**. Black dots mark sampling locations of CH_3I observations (shown in Fig. 1).

BGD
10, 17549–17595, 2013

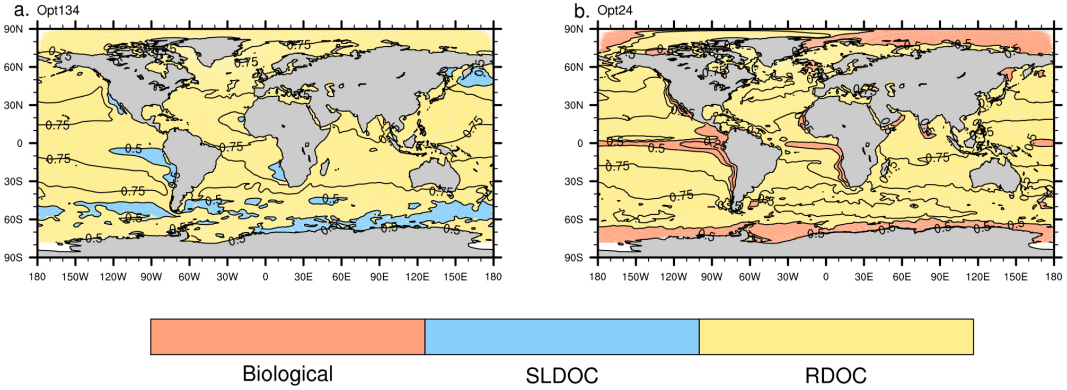

Fig. 7. Source apportionment (shaded contours: local dominant source, black contour lines: fraction of photochemical production from RDOC) in the experiment with mixed biological and photochemical production, Opt134, **(a)** and the one with mixed biological production considering stressed picocyanobacteria and photochemical production from RDOC, Opt24, **(b)**.

BGD
10, 17549–17595, 2013

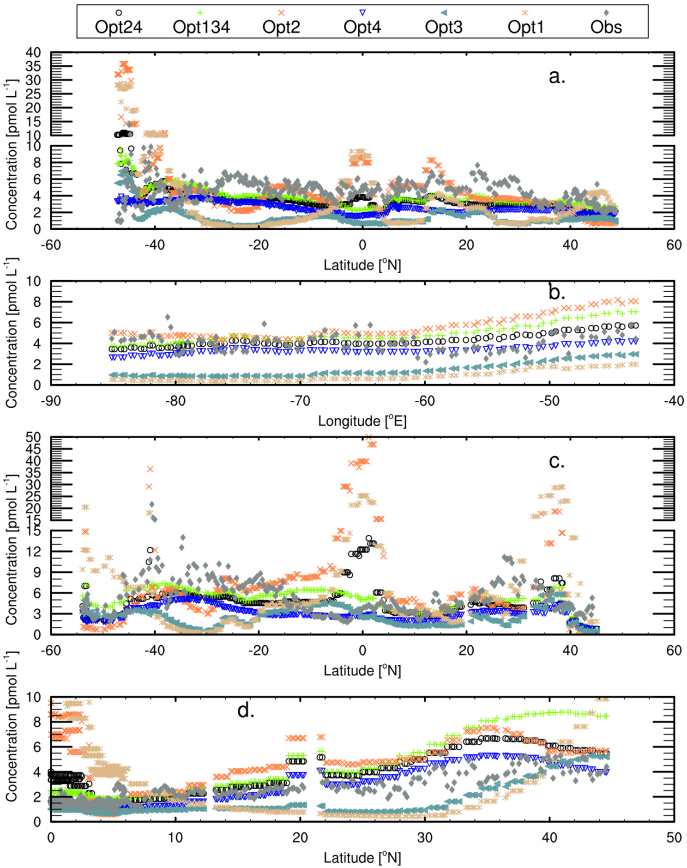

Fig. 8. Observed and modelled methyl iodide concentrations [pmol L^{-1}]. Observations are from Butler et al. (2007) (**a** Blast 2, **b** Gas Ex 98, **c** Blast 1, **d** Phase 1-04, see also Figs. S1, S8, S10, and S11), Note the broken y-axes in **(a)** and **(c)**.

BGD
10, 17549–17595, 2013

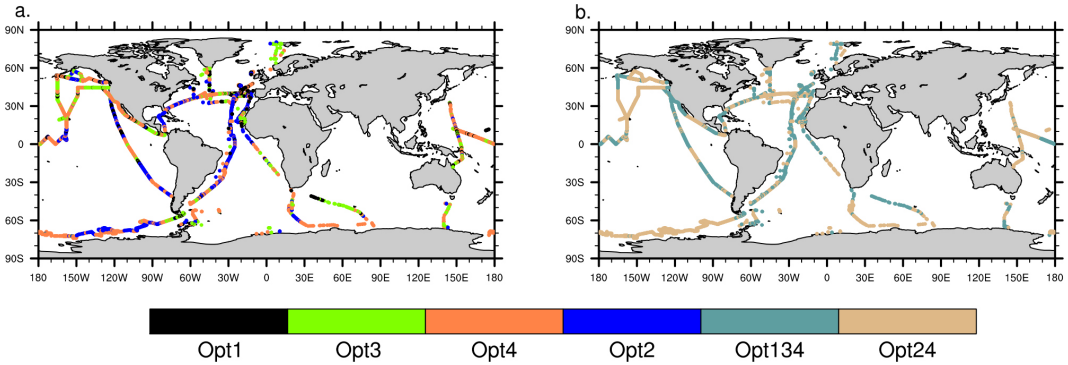

Fig. 9. Experiment closest to the observed concentration at the sea surface, when considering only single-source experiments **(a)**, only mixed-source experiments **(b)**.

BGD
10, 17549–17595, 2013

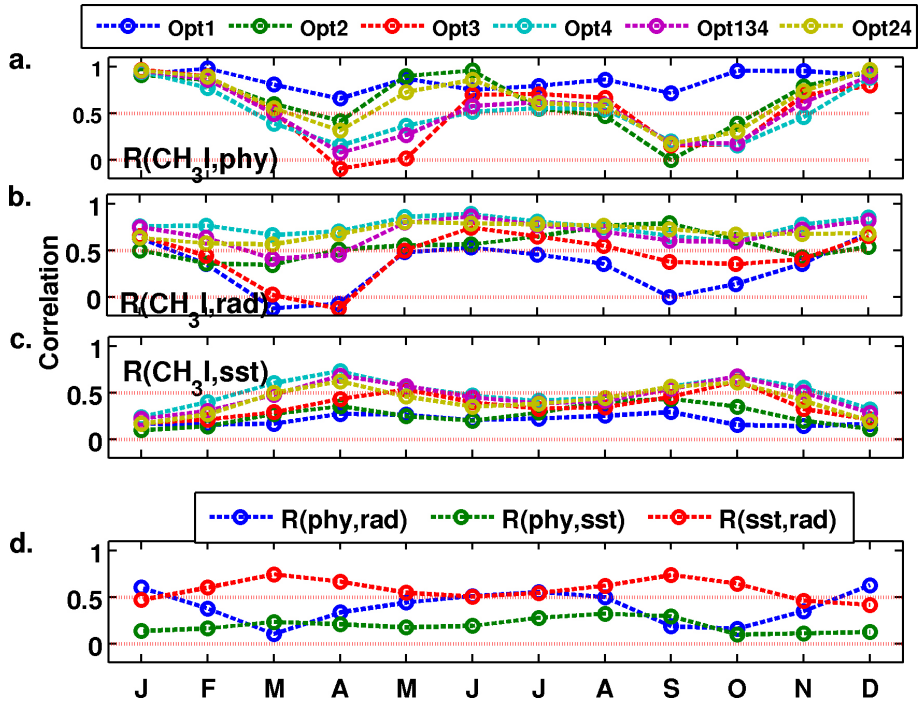

Fig. 10. Spatial correlation of the monthly methyl iodide surface concentrations along the 30 W meridian (60N-60S) with surface phytoplankton concentrations **(a)**, radiation **(b)** and sea surface temperature **(c)**, and spatial correlations of phytoplankton and radiation (R(phy, rad)), phytoplankton and SST (R(phy, sst)), and SST and radiation (R(sst, rad)) **(d)**. All correlations are significant on the 95 % level.

BGD
10, 17549–17595, 2013

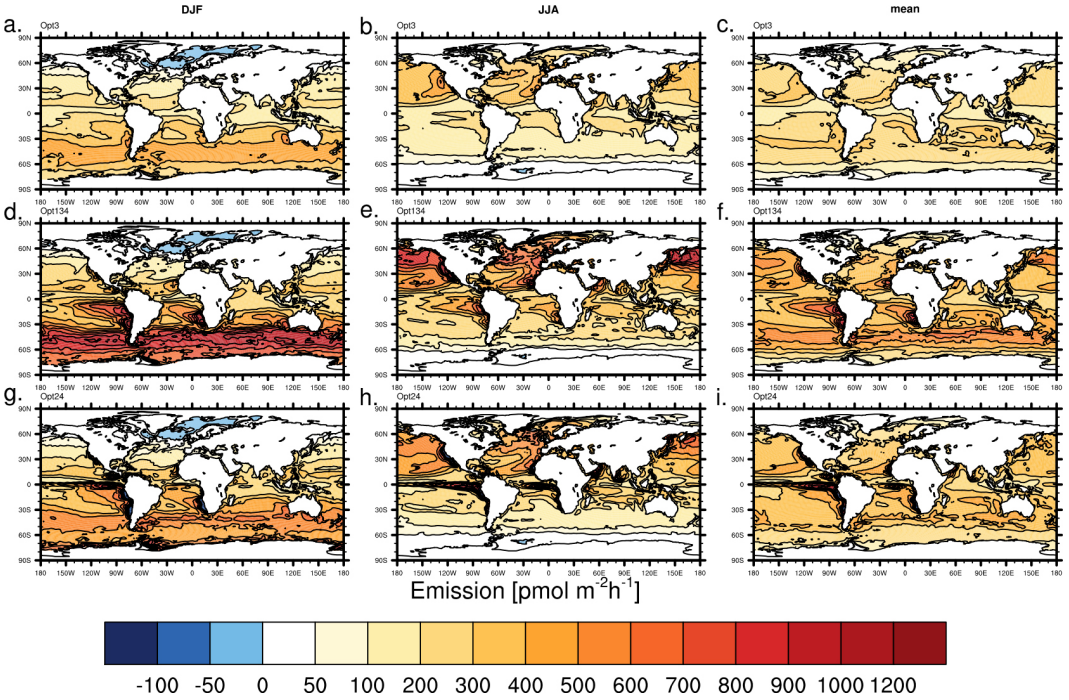

Fig. 11. Emissions to the atmosphere [pmol $m^{-2} h^{-1}$] in Opt4 **(a–c)**, Opt134 **(d–f)**, Opt24 **(g–i)** in DJF **(a, e, i)**, in JJA **(c, g, k)**, annual mean **(c, f, i)**.

BGD
10, 17549–17595, 2013